Chiral emission of electric dipoles coupled to optical hyperbolic materials

Wenxiao Liu,[1,2] Vinod M. Menon,[3] Shaoyan Gao,[1,*] and Girish S. Agarwal[2,†]

[1]*Shaanxi Province Key Laboratory for Quantum Information and Quantum Optoelectronic Devices, and Department of Applied Physics, Xi'an Jiaotong University, Xi'an 710049, China*

[2]*Institute for Quantum Science and Engineering, and Department of Biological and Agricultural Engineering, Texas A&M University, College Station, Texas 77843, USA*

[3]*Department of Physics, City College of New York, 160 Convent Ave., New York, New York 10031, USA*

(Received 30 September 2019; revised manuscript received 27 November 2019; published 23 December 2019)

We examine the directional characteristics of emission from a dipole on hyperbolic metamaterial (HMM) and we show the possibility of chiral emission which is strongly dependent on the polarization of the dipole. Using rigorous solutions of the Maxwell equations, we present analytical results on chirality which depends on the excitation of different evanescent modes in the HMM, some of which are easily accessible in current experiments. The origin of chirality lies in the near field interference of emission arising from parallel and perpendicular components of the dipole polarization especially if the two polarizations are out of phase by $\pi/2$. The dependence of chirality on the distance of the dipole from the HMM is obtained. The truly unidirectional emission is possible for some specific complex elliptic polarization of the dipole. Our analysis is based on the Green's function for the multilayered HMM. We also present results on chiral emission from emitters on metal surfaces. These results provide opportunities for controlling the excitation of the surface waves and can have potential applications in sensing molecules on HMM surfaces.

DOI: 10.1103/PhysRevB.100.245428

I. INTRODUCTION

Interaction of chiral light with matter has received much interest lately due to the potential applications ranging from quantum information processing [1–5] to bio-sensing [6,7]. The realization of chiral coupling depends on propagation direction of electromagnetic waves and polarization-dependent transitions of quantum emitters. When illuminating nanophotonic structures, such as nanofibers [8,9] and plasmonic waveguides [10–12], by an excitation beam with circular polarization, optical spin-momentum locking effects can be exploited to control propagation direction [13–18]. Several strategies have been proposed to directly launch surface plasmon modes, for instance, by using asymmetric slanted grating [10] or illuminating a nearby nanoantenna [11,19]. Moreover, near-field interferences induced by circularly polarized dipoles provide another approach for directional excitation of guided modes with broadband properties [12].

Various anisotropic metamaterials [20–23], especially bulk uniaxial hyperbolic media, have been recently exploited to realize directional excitation with transverse light localization. Hyperbolic metamaterials (HMM) have opposite signs in the longitudinal and tangential dielectric permittivities, and these guided modes in HMMs exhibit hyperbolic dispersion [20,21]. Moreover, HMMs support broadband enhanced density of states and extremely large vectors [24], which allow them to achieve broadband enhanced spontaneous emission [25–35], subdiffraction imaging [36], negative refraction [37–39], long-range energy transfer [40,41], and directional single photon emission [42]. These applications are restricted by Ohmic losses of the metal and nonlocal effects originating from the subwavelength unit cell [43,44]. In general, they can be artificially fabricated by layered metal-dielectric structures or nanowire arrays. Directional excitation of phonon polaritons in 2D materials with hyperbolic dispersion was demonstrated theoretically [22,45]. A recent experiment showed the directional routing effect at radio frequencies in HMMs consisting of lumped elements [16].

Recently, monolayer semiconductors, such as monolayer transition-metal dichalcogenides (TMD) and quantum dots, have emerged as a new material platform for studying light-matter interaction. Particularly, the broken inversion symmetry and strong spin-orbit interaction present in TMDs contribute to valley-dependent optical selection rule. With the help of a metasurface, valley-selective emission and spontaneous valley coherence in TMDs have been demonstrated in experiment and theory [46–48]. The TMDs and quantum dots can be considered as a local in-plane excitonic dipole with different polarizations [49,50]. Here, we investigate the emission characteristics of an electric dipole placed near a dielectric-metal multilayered structure. By tuning the polarization handedness of an elliptical polarized dipole, directional and unidirectional emission can be realized. The emission patterns have narrow bandwidth in HMMs around directions determined by the system parameters. This work is motivated by experiments from two different groups: (i) The possibility of chiral selective emission was realized by the valley excitons of TMDs coupled to the HMMs [51]. (ii) Directional and chiral emission was seen in experiments on quantum dots coupled to the evanescent modes of the HMMs [52].

*Corresponding author: gaosy@mail.xjtu.edu.cn
†Corresponding author: girish.agarwal@tamu.edu

 ©2019 American Physical Society

The paper is organized as follows: In Sec. II, by using the method of photon Green's function, we briefly describe the elementary theory for the interaction of a dipole coupled to a dielectric-metal multilayered structure. We discuss the anomalous transmission across a HMM by comparison with effective medium theory and transfer matrix method. In Sec. III, we present numerical results of chiral emission by tuning the polarization handedness of the dipole. The analytic expressions for chiral emission are given in Sec. IV. The results of chiral emission for a single unit of the HMMs are given in Sec. V. In Sec. VI, we demonstrate the influences of the distance of the dipole from the multilayered structure on the chirality, followed by conclusions in Sec. VII.

II. DIPOLAR FIELD DISTRIBUTION USING GREEN'S FUNCTION

Here, we provide the theory of the interaction between light in a multilayered structure and a quantum emitter with a two-dimensional polarization state. We assume that the multilayered structure is strictly planar so that s and p polarizations do not couple with each other. Any surface disorder can produce this coupling [53]. We have currently ignored such a surface disorder as in the experiment of Ref. [51], one did not observe any evidence of such a disorder induced coupling. Additionally, the surface roughness of these HMM films is under 1 nm as was shown previously [34]. In the presence of strong surface disorder, hybrid plasmon polaritons can occur [45,54,55]. The schematic of the proposed setup is depicted in Fig. 1, considering that the emitter, such as quantum dots, is located at $\mathbf{r}_0 = (x_0, y_0, z_0)$ on the upper surface of the multilayered structure. Typically, an emitter in nature can be treated as an elliptically polarized electric dipole. The electric dipole moment is $\mathbf{p}_a = p_0[\cos(\theta)\mathbf{x} + i\sin(\theta)\mathbf{z}]$, where p_0 is the amplitude and the angle θ is measured with respect to the $+x$ axis. The total height between the layered interfaces is d. The electric field at $\mathbf{r} = (x, y, z)$ in the lower half space, in the region of substance, can be calculated by [56]

$$\mathbf{E}(\mathbf{r}) = \omega^2 \mu\mu_0 \overleftrightarrow{\mathbf{G}}(\mathbf{r}, \mathbf{r}_0) \cdot \mathbf{p}_a, \tag{1}$$

where μ_0 is the permeability in vacuum. The materials we consider here are nonmagnetic with the permeability $\mu = 1$. In the angular spectrum representation, the scattered electric Green's function consisting of transmission waves is given by

$$\overleftrightarrow{\mathbf{G}}(\mathbf{r}, \mathbf{r}_0) = \frac{i}{8\pi^2} \iint_{-\infty}^{\infty} (\overleftrightarrow{\mathbf{M}}^{s} + \overleftrightarrow{\mathbf{M}}^{p}) e^{i[k_x(x-x_0)+k_y(y-y_0)]} \times e^{i[-k_{zn}(z+d)+k_{z1}z_0]}\, dk_x dk_y, \tag{2}$$

where

$$\overleftrightarrow{\mathbf{M}}^{s} = \frac{t^{s}(k_x, k_y)}{k_{z1}(k_x^2 + k_y^2)} \begin{pmatrix} k_y^2 & -k_x k_y & 0 \\ -k_x k_y & k_x^2 & 0 \\ 0 & 0 & 0 \end{pmatrix}, \tag{3a}$$

$$\overleftrightarrow{\mathbf{M}}^{p} = \frac{t^{p}(k_x, k_y)}{k_1 k_n (k_x^2 + k_y^2)} \times \begin{pmatrix} k_x^2 k_{zn} & k_x k_y k_{zn} & \frac{k_x (k_x^2+k_y^2) k_{zn}}{k_{z1}} \\ k_x k_y k_{zn} & k_y^2 k_{zn} & \frac{k_y (k_x^2+k_y^2) k_{zn}}{k_{z1}} \\ k_x (k_x^2 + k_y^2) & k_y (k_x^2 + k_y^2) & \frac{(k_x^2+k_y^2)^2}{k_{z1}} \end{pmatrix}. \tag{3b}$$

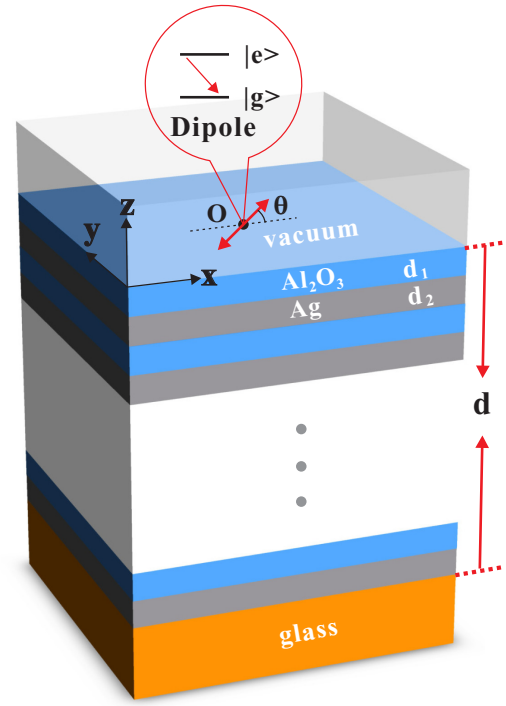

FIG. 1. Schematic of a dipole deposited on the surface of a three-dimensional hyperbolic metamaterial. The hyperbolic metamaterial consists of alternating layers of Al_2O_3 and silver with a total thickness $d = 140$ nm. The inset circle shows the energy level diagram of a quantum emitter.

In these equations, k_x (k_y) is the x (y) component of the wave vector, and k_{z1} and k_{zn} are the z component of the wave vectors in the vacuum ($k_1 = \omega/c$) and in the substance ($k_n = \sqrt{\epsilon_n}\omega/c$), respectively. Note that t_s and t_p are transmission coefficients of s-polarized and p-polarized waves, respectively. For simple configurations, they can be obtained by using Fresnel equations. However, in the multilayered structure the transfer matrix method (TMM) is required to calculate the exact results. For an N-layer structure with each layer dielectric constant ϵ_i and thickness d_i, the general expression is given by [25]

$$\begin{pmatrix} 1 \\ r^{s,p} \end{pmatrix} = \left(D_0^{s,p}\right)^{-1} T^{s,p} D_{N+1}^{s,p} \begin{pmatrix} t^{s,p} \\ 0 \end{pmatrix}, \tag{4}$$

where

$$T^{s,p} = \prod_{i=1}^{N} D_i^{s,p} P_i \left(D_i^{s,p}\right)^{-1}, \quad D_i^{s} = \begin{pmatrix} 1 & 1 \\ k_{zi} & -k_{zi} \end{pmatrix}, \tag{5a}$$

$$D_i^{p} = \begin{pmatrix} 1 & 1 \\ \frac{k_{zi}}{\epsilon_i} & -\frac{k_{zi}}{\epsilon_i} \end{pmatrix}, P_i = \begin{pmatrix} e^{-ik_{zi}d_i} & 0 \\ 0 & e^{ik_{zi}d_i} \end{pmatrix}. \tag{5b}$$

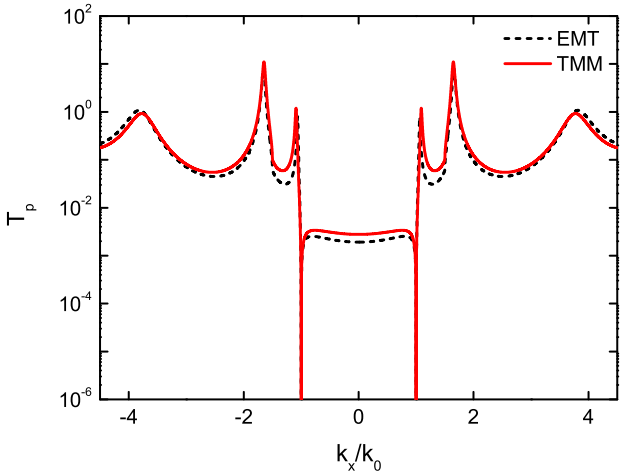

FIG. 2. Comparison of the effect medium theory (EMT) and transfer matrix method (TMM). The transmission coefficient $|t_p|^2$ of p-polarized waves versus the wave vector component k_x across the hyperbolic metamaterial for $d = 140$ nm and $k_y = 0$.

Equations (4) and (5) allow us to calculate the transmission spectra across a multilayered structure. In particular, the poles of transmission coefficients correspond to the eigenmodes for the considered structure. Combining all of these results, the electromagnetic field distribution and the local density of states induced by a dipole in the lower space of a multilayered structure can be obtained.

As described in Eqs. (1) and (2), the electric field has a form of spatial Fourier integral (Sommerfeld integral), which needs to be solved by using numerical integration techniques. For convenience, in the following we consider the Fourier amplitude spectrum with $\mathbf{E}(k_x, k_y) = \frac{i\omega^2\mu\mu_0}{2} e^{i[-k_{zn}(z+d)+k_{z1}z_0]}(\overleftrightarrow{\mathbf{M}}^{\mathrm{s}} + \overleftrightarrow{\mathbf{M}}^{\mathrm{p}}) \cdot \mathbf{p}_{\mathrm{a}}$. The electric field densities can be expressed as

$$|\mathbf{E}(k_x, k_y)|^2 = \left(\frac{\omega^2\mu\mu_0 \mathrm{p}_0}{2}\right)^2 I, \tag{6}$$

where

$$I = |e^{(i[-k_{zn}(z+d)+k_{z1}z_0])}|^2 \cdot [|\mathbf{M}_{xx}\cos(\theta) + i\mathbf{M}_{xz}\sin(\theta)|^2 + |\mathbf{M}_{zx}\cos(\theta) + i\mathbf{M}_{zz}\sin(\theta)|^2], \ \overleftrightarrow{\mathbf{M}} = \overleftrightarrow{\mathbf{M}}^{\mathrm{s}} + \overleftrightarrow{\mathbf{M}}^{\mathrm{p}}, \tag{7}$$

and where θ gives the orientation of the dipole with dipolar moment $\mathbf{p}_{\mathrm{a}} = \mathrm{p}_0[\cos(\theta)\mathbf{x} + i\sin(\theta)\mathbf{z}]$. Note that the expression for electric field distribution includes the contribution of the propagating ($\kappa < k_0$) and evanescent ($\kappa > k_0$) waves, where $\kappa = \sqrt{k_x^2 + k_y^2}$.

Let us focus on a concrete example. We consider that a multilayered hyperbolic metamaterial (HMM) consists of alternating layers of Al_2O_3 and silver with a total thickness $d = 140$ nm, as shown in Fig. 1. Each single layer of Al_2O_3 and silver has the same thickness with $d_1 = d_2 = 10$ nm. The upper substrate we assume is vacuum with the permittivity ϵ_0. The relative dielectric constant of the glass substrate is $\epsilon_{\mathrm{g}} = 2.25$. For the incident wavelength $\lambda = 615$ nm, the relative dielectric constants of Ag and Al_2O_3 are $\epsilon_{\mathrm{Ag}} = -15.6143 + 2.162i$ and $\epsilon_{\mathrm{Al_2O_3}} = 3.1223$, respectively. Typically, the HMMs can be described as a uniaxial medium with a diagonal permittivity tensor ($\epsilon_x = \epsilon_y = \epsilon_\parallel$, $\epsilon_z = \epsilon_\perp$, and $\epsilon_\parallel \neq \epsilon_\perp$). The optical axis is perpendicular to the interfaces and along the direction of the z axis.

Generally, the effective permittivities $(\epsilon_\parallel, \epsilon_\perp)$ of the HMMs are determined by the geometry and material properties of individual components. In this case, within the effective medium theory (EMT) they can be given by $\epsilon_\parallel = p\epsilon_{\mathrm{Ag}} + (1-p)\epsilon_{\mathrm{Al_2O_3}}$ and $\epsilon_\perp = [p/\epsilon_{\mathrm{Ag}} + (1-p)/\epsilon_{\mathrm{Al_2O_3}}]^{-1}$, with a filling fraction $p = d_2/(d_1 + d_2)$. Under the above conditions, we have $\epsilon_\parallel = -6.246 + 1.081i$ and $\epsilon_\perp = 7.76 + 0.2624i$, which defines the medium as a type-II hyperbolic metamaterial ($\epsilon_\parallel < 0$ and $\epsilon_\perp > 0$). Therefore, the isofrequency curve of the HMMs is a one-sheeted hyperboloid. They usually support two types of waves: ordinary and extraordinary ones. The transmission coefficients can be expressed as

$$t_{\mathrm{s}} = \frac{4k_{z1}k_{zo}e^{ik_{zo}d}}{(k_{zo}+k_{z1})(k_{zo}+k_{zn}) - (k_{zo}-k_{z1})(k_{zo}-k_{zn})e^{2ik_{zo}d}}, \tag{8a}$$

$$t_{\mathrm{p}} = \frac{4k_{z1}k_{ze}\epsilon_{\mathrm{n}}\epsilon_\parallel e^{ik_{ze}d}}{(k_{ze}+\epsilon_\parallel k_{z1})(\epsilon_{\mathrm{n}}k_{ze}+\epsilon_\parallel k_{zn}) - (k_{ze}-\epsilon_\parallel k_{z1})(\epsilon_{\mathrm{n}}k_{ze}-\epsilon_\parallel k_{zn})e^{2ik_{ze}d}}. \tag{8b}$$

The wave vector components for the ordinary and extraordinary modes in the z direction are given by $k_{zo} = \sqrt{k_0^2\epsilon_\parallel - \kappa^2}$ and $k_{ze} = \sqrt{k_0^2\epsilon_\parallel - \frac{\epsilon_\parallel}{\epsilon_\perp}\kappa^2}$. In our case the s and p polarized waves do not mix as the optic axis of the effective uniaxial [anisotropic] medium is perpendicular to the interface. However at the interface of the uniaxial anisotropic medium and an isotropic medium the Dyakonov surface waves can exist [54,55]. These are localized hybrid TE and TM waves and are most prominent if the optic axis of the positive uniaxial medium is in the plane of the interface.

Before discussing dipolar emission characteristics, we examine the anomalous transmission ($T_p = |t_p|^2$) across the HMMs for the case of $k_y = 0$, as shown in Fig. 2. The calculation by using effective medium theory can match well with that of transfer matrix method, with slight deviations in values of peaks. Different coupled surface modes are present in HMMs, corresponding to multiple peaks at positions $k_x/k_0 = \pm 1.088, \pm 1.648$, and ± 3.774. The transmission is symmetric along the axis $k_x = 0$, which means that these eigenmodes in HMMs are bidirectional propagation. For the propagating waves ($k_x < k_0$), free electron motion in type-II HMMs greatly contributes to the overall reflection and results in the transmission (T_p) near to zero [57]. However, for high-k evanescent waves ($k_x > k_0$), the transmission (T_p) can be larger than 1 due to the enhanced photonic density of

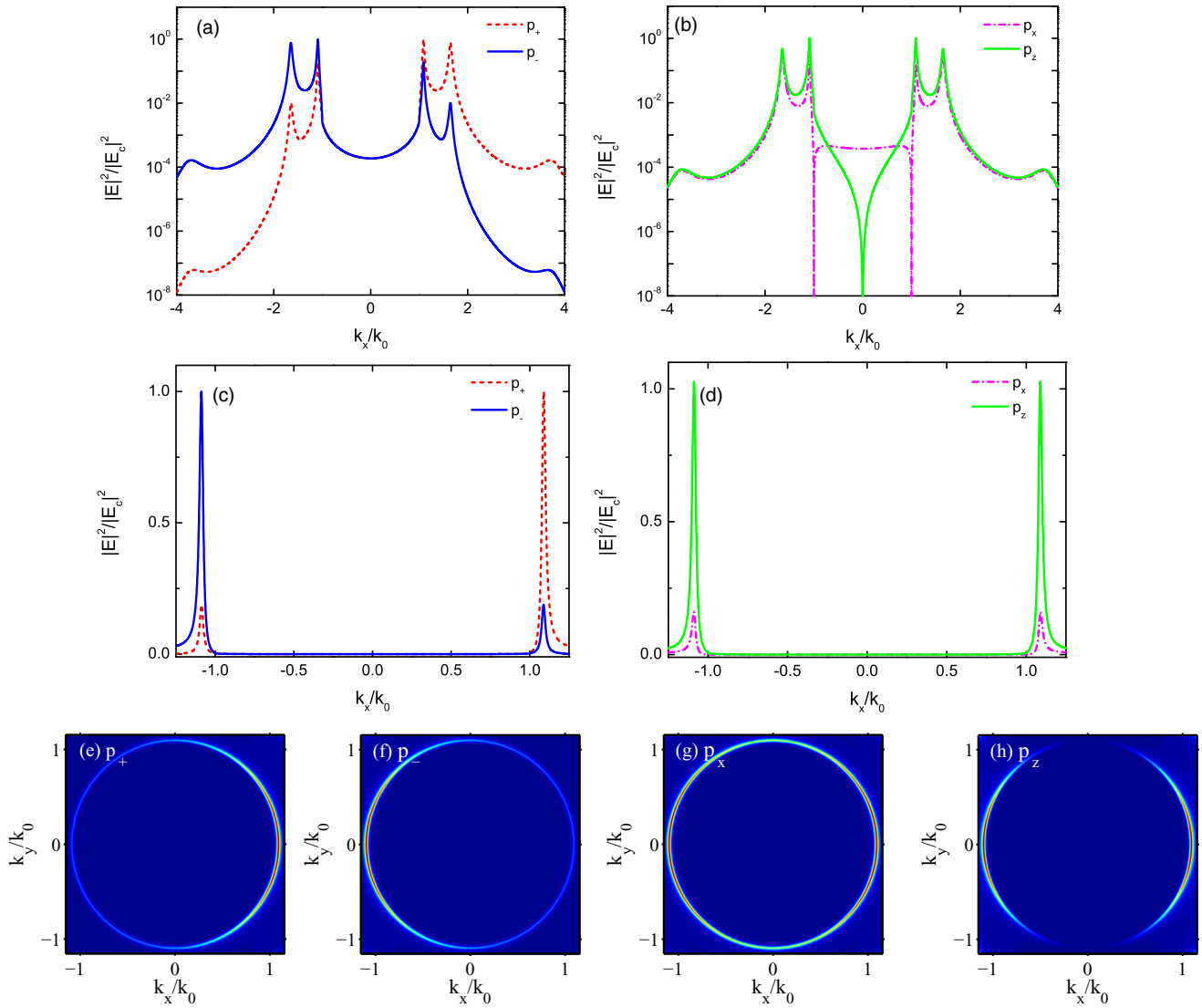

FIG. 3. Electric field intensity distributions on the lower surface of the hyperbolic metamaterial induced by circularly polarized (a),(c) and linearly polarized (b),(d) dipoles with $k_y = 0$. The electric field E_c used for normalization corresponds to the larger peak value induced by the circular polarized dipole in (c). (e)–(h) Field maps $|E|^2/|E_{\max}|^2$ excited by an electric dipole $\mathbf{p}_a = p_0[\cos(\theta)\mathbf{x} + i\sin(\theta)\mathbf{z}]$, with (e) $\theta = \pi/4$, (f) $\theta = -\pi/4$, (g) $\theta = 0$, and (h) $\theta = \pi/2$.

states, which is induced by the coupling between the short-range surface plasmon polaritons in metal layers [58]. The maximum of the transmission in this case is 11.06. By adding more metal layers, the eigenmodes present in the multilayered structure can increase in number due to coupled plasmonic states. However, when a dipole is placed close to the surface of the HMMs, effective medium theory will be not applicable due to the breakdown of homogeneous effective medium approximation [28,29,31,59]. Furthermore, effective medium theory cannot give an explanation to the ordering of the layers. Therefore, in the following we will utilize full transfer matrix calculations to obtain the transmission coefficients of the multilayered structures.

III. CHIRAL EMISSION FROM POLARIZED DIPOLES ON HMMS

We now study the effects of polarization handedness of a dipole on the chiral emission. When the wave vector component $k_y = 0$, we can find that s-polarized waves have no contribution to the electric field from Eqs. (3a) and (7). Furthermore, for the x component of the electric field, we have a relationship with $E_x \propto \mathbf{M}^{\mathrm{p}}_{xx}\cos(\theta) + i\mathbf{M}^{\mathrm{p}}_{xz}\sin(\theta)$, which is a linear superposition of the vertical and horizonal oriented components of the dipole. For evanescent waves with $|k_x| > k_0$, the term k_{z1} makes $\mathbf{M}^{\mathrm{p}}_{xz}$ be a complex number. Consequently, the relation can be reduced to $E_x \propto \cos(\theta) + \sin(\theta)k_x/|k_{z1}|$. If $0 < \theta < \pi/2$, the spectral amplitudes with $k_x < -k_0$ add up destructively, whereas for $k_x > k_0$ constructive interference occurs. The electric field intensity has a relation with $I_x^p \propto [\cos(\theta) + \sin(\theta)k_x/|k_{z1}|]^2$. However, if we let the dipolar moment be $\mathbf{p}_a = p_0[\cos(\theta)\mathbf{x} + \sin(\theta)\mathbf{z}]$ without a $\pi/2$ phase difference in the x and z direction, the electric field intensity for evanescent waves can be written as $I_x^p \propto \cos^2(\theta) + [\sin(\theta)k_x/|k_{z1}|]^2$. There is no interference phenomenon in this case. Therefore, we emphasize that the phase in dipolar moment is important for the chiral emission.

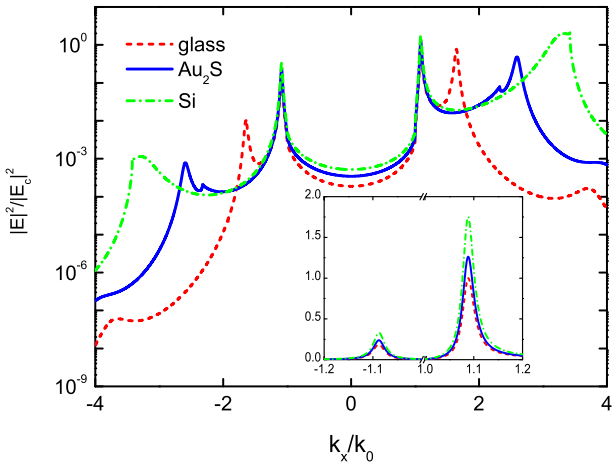

FIG. 4. Plot of $|E|^2/|E_c|^2$ versus the wave vector component k_x excited by a dipolar emitter with circular polarization ($\mathbf{p}_+$) for different substances. The dielectric constants of glass, Au_2S, and silicon are $\epsilon_g = 2.25$, $\epsilon_{Au_2S} = 5.4$, and $\epsilon_{Si} = 11.7$, respectively. Here, $k_y = 0$.

In Figs. 3(a)–3(d), we present the electric field intensities in the lower space when the HMMs is excited by linearly polarized dipoles and circularly polarized dipoles. The poles of the spatial frequency spectra do not depend on the polarization of the dipole, but rely on the geometry and material properties, which is determined by the denominator of the transmission coefficient. For linearly polarized cases $\mathbf{p}_x$ or $\mathbf{p}_z$ ($\theta = 0$ or $\theta = \pi/2$), the frequency spectra are symmetric, which means that there is no preference in the coupling with forward or backward modes. However, for circularly polarized dipoles with $\mathbf{p}_\pm = (\mathbf{x} \pm i\mathbf{z})/\sqrt{2}$, the superposition of the horizontal and longitudinal component of the dipole results in the near-field interference, leading to a nonsymmetric spatial-frequency spectra. For a right-circularly polarized dipole ($\mathbf{p}_+$), the incident field couples more efficiently with the forward-propagating mode for $k_x > k_0$. For a left-circularly polarized dipole ($\mathbf{p}_-$), the incident field couples more efficiently with the backward-propagating mode for $k_x < -k_0$. In Figs. 3(c) and 3(d), the spectra have a narrow bandwidth at around $k_x/k_0 = \pm 1.088$ and the qualitative results can be inferred for different polarization handedness. Moreover, the intensity maps plotted in Figs. 3(e)–3(h) contain information for both TE and TM modes along the k_x and k_y direction. Note that there is no preference in the k_y direction. This is because for $k_x = 0$, $\mathbf{M}^{s}_{xx}$ and $\mathbf{M}^{p}_{zz}$ are even functions of k_y. For the circularly polarized dipoles, the asymmetry of the electric intensity appears in the k_x direction for different k_y as described above. We stress that by using a circularly polarized dipole, the completely effective unidirectional excitation cannot be realized.

As discussed above, the evanescent wave plays a great role in the near field interference. This is similar to the spin Hall effect [18,60–62]. When an elliptically polarized dipole illuminates a multilayered plasmonic structure, the inversion symmetry is broken and the high-wave vector modes can be excited. The evanescent modes carry transverse spin angular momentum [18,60,61], whose sign only relies on the propagation direction. Therefore, the best coupling can be achieved when the transverse spin of the evanescent mode matches

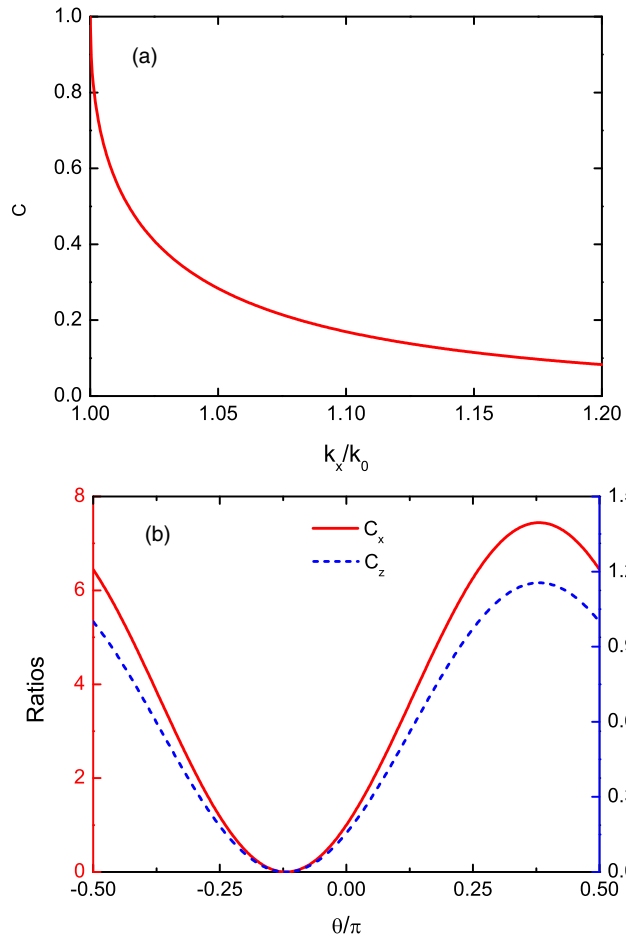

FIG. 5. The intensity ratio C (a) as a function of the wave vector component k_x. The intensity ratios C_x and C_z (b) at $k_x/k_0 = 1.088$ as a function of the angle θ. Here, $k_y = 0$ and $k_x > k_0$.

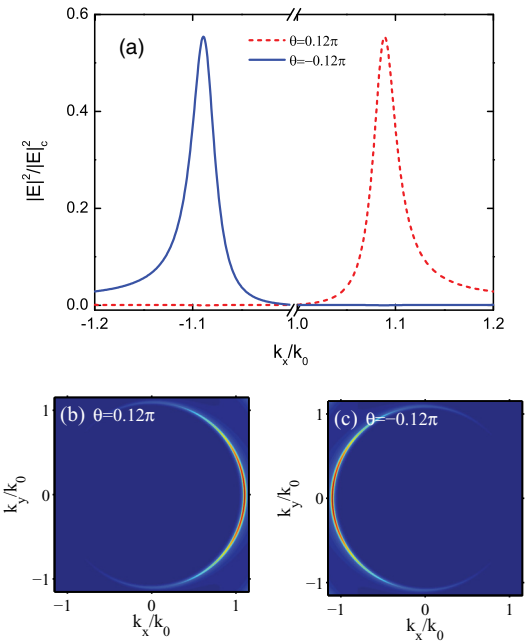

FIG. 6. (a) Electric field intensity $|E|^2/|E_c|^2$ versus the wave vector component k_x for $\theta = \pm 0.12\pi$. Here, we set $k_y = 0$. (b),(c) The corresponding electric field maps $|E|^2/|E_{max}|^2$.

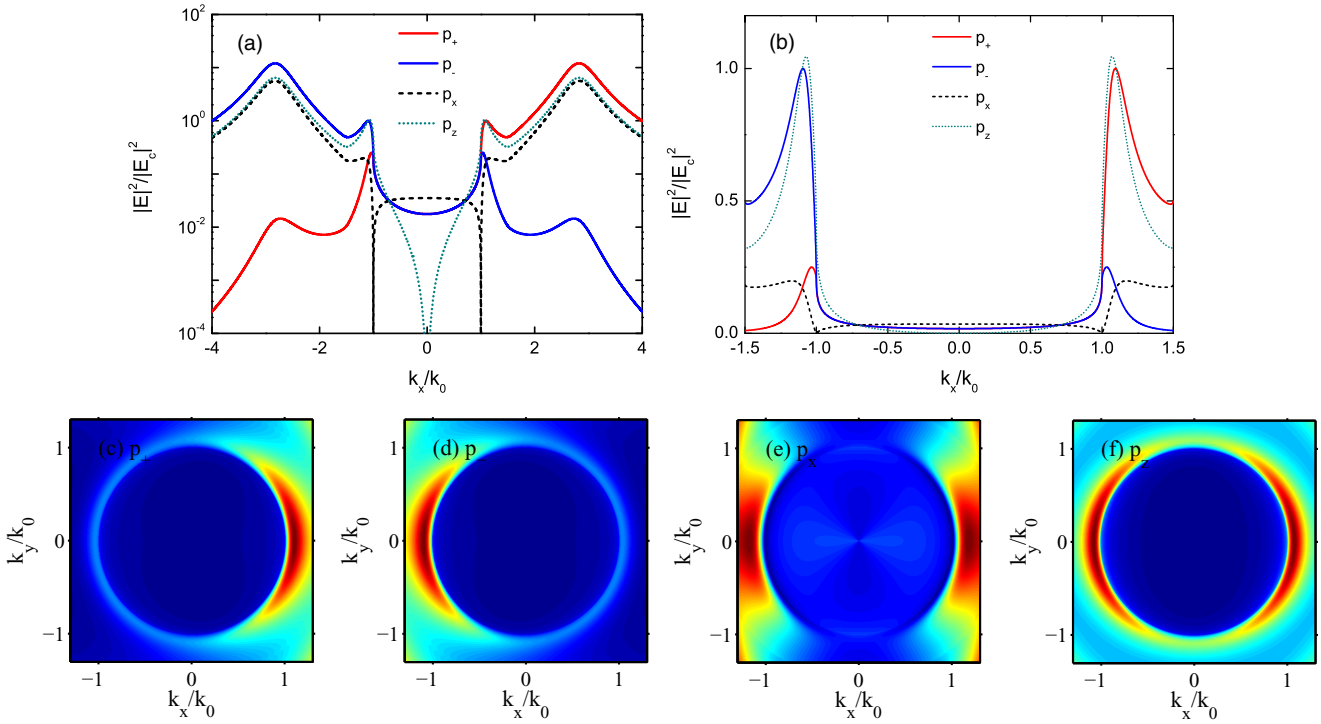

FIG. 7. Electric field intensity distribution as a function of the wave vector component k_x across the vacuum/Al_2O_3/Ag/glass multilayered structure excited by circularly polarized and linearly polarized dipoles (a),(b) with $k_y = 0$. The electric field E_c used for normalization corresponds to the larger peak value induced by the circular polarized dipole in (b). (c)–(f) Field maps $|E|^2/|E_{max}|^2$ excited by a dipole $\mathbf{p}_a = p_0[\sin(\theta)\mathbf{x} + i\cos(\theta)\mathbf{z}]$, with (c) $\theta = \pi/4$, (d) $\theta = -\pi/4$, (e) $\theta = 0$, and (f) $\theta = \pi/2$.

with the spin of the incident field, i.e., the wave vector in plane parallel to polarized direction of the dipole. By tuning the polarization handedness of the dipole, the excitation and guidance of electromagnetic modes in a nanostructure can be controlled [12].

Figure 3 shows the excitation of evanescent modes corresponding to high values of k_x. It is possible to access these by using a substrate with higher refractive index. The influence of refractive index of the lower base material on the electric field distribution induced by a right-circularly polarized dipole are presented in Fig. 4. When increasing the refractive index of the substance, the spectra also display an asymmetric profile with a reduction in number of eigenmodes. Moreover, the sideband peaks for ($|k_x| > 1.1k_0$) show a redshift to higher wave vectors. At about $k_x/k_0 = \pm 1.088$, though the intensity is enhanced, the intensity ratio seems not to change. High refractive index medium increases the local density of states and then can be utilized to modify the emission pattern.

IV. ANALYTICAL EXPRESSIONS FOR CHIRALITY

In the following, we give the exact expression of Eq. (7) to analyze the quantitative relation induced by different dipolar polarization states. When $k_y = 0$, the electric field intensity excited by the dipole ($\mathbf{p}_a$) can be described as

$$I^{\mathrm{p}} = \left| e^{-ik_g d} \frac{t^p(k_x)}{k_0} \right|^2 \left| \cos(\theta) + i\sin(\theta)\frac{k_x}{k_{z1}} \right|^2, \tag{9}$$

where $k_{z1} = k_0\sqrt{1-(k_x/k_0)^2}$. For the circularly polarized dipoles, we have unit polarization vectors $\mathbf{p}_\pm = (\mathbf{x} \pm i\mathbf{z})/\sqrt{2}$ corresponding to $\theta = \pm\pi/4$. The unit vectors of the horizontally and vertically polarized dipoles are $\mathbf{p}_x = \mathbf{x}$ and $\mathbf{p}_z = \mathbf{z}$ corresponding to $\theta = 0$ and $\theta = \pi/2$, respectively. We first define the intensity ratio contributed by the evanescent waves ($k_x > k_0$) between the left-circularly and right-circularly polarized components by

$$C = \frac{I^{\mathrm{p}}|_{\mathbf{p}_-}}{I^{\mathrm{p}}|_{\mathbf{p}_+}} = (\gamma - \sqrt{\gamma^2 - 1})^4, \tag{10}$$

where $\gamma = k_x/k_0 > 1$. We also can obtain the intensity ratios induced by the elliptically and linearly polarized dipoles,

$$C_x = \frac{I^{\mathrm{p}}}{I^{\mathrm{p}}|_{\mathbf{p}_x}} = \left[\cos(\theta) + \frac{\sin(\theta)}{\sqrt{1-1/\gamma^2}}\right]^2, \tag{11}$$

$$C_z = \frac{I^{\mathrm{p}}}{I^{\mathrm{p}}|_{\mathbf{p}_z}} = [\cos(\theta)\sqrt{1-1/\gamma^2} + \sin(\theta)]^2. \tag{12}$$

By using these theoretical formulations, we can study how to control the excitation direction of electric field by tuning the polarization of the dipolar emitter.

In Fig. 5(a), we present the intensity ratio C between the left-circularly and right-circularly polarized components as a function of the wave vector component k_x for $k_x > k_0$. With increasing the wave vector component k_x, the intensity ratio C monotonically decreases. For $k_x/k_0 = 1.088$, we have $C = 0.189$, which denotes that the circularly polarized dipole does not provide efficient unidirectional excitation. We also

plot the intensity ratios C_x and C_z as a function of the angle θ for $k_x/k_0 = 1.088$ in Fig. 5(b). For $\theta = 0$ (a x-polarized dipole), we can obtain $C_x = 1$ and $C_z = 0.155$. For $\theta = \pm\pi/2$ (a z-polarized dipole), we get $C_x = 6.443$ and $C_z = 1$. The contribution of the x-polarized dipole to the electric field is much lower than that of the z-polarized dipole. With increasing the angle θ, the ratios C_x and C_z first go down to zero at $\theta = -0.12\pi$. Then they grow up and reach a maximum at $\theta = 0.38\pi$. Finally they decrease again. The case for $\theta = -0.12\pi$ implies a truly unidirectional excitation of the electromagnetic wave. This behavior can be clearly observed in Fig. 6, with no coupling to the forward (backward) propagating mode at $k_x/k_0 = 1.088$ ($k_x/k_0 = -1.088$). By tuning the polarization handedness, we can control the contribution for the proportion of the x-polarized and z-polarized components to the electric field and realize the directional excitation where the electric field is suppressed in one direction.

V. RESULTS FOR CHIRAL EMISSION FROM POLARIZED DIPOLES AT A SINGLE UNIT OF HMM

In this section, we study the possibility of realizing the chiral emission by using a vacuum/Al_2O_3/Ag/glass multilayered structure with $d = 20$ nm ($d_1 = d_2 = 10$ nm). We present the simulated electric field intensities when a dipole with the linear or circular polarization is on the surface of the multilayered structure, as shown in Fig. 7. Similar behaviors can be observed by comparison to those in the HMMs. However, in this case, in the region of propagating waves ($|k_x| < k_0$), the electric field is much larger due to the transmission $|t_p|^2 \simeq 1$. The eigenmodes have a broad bandwidth due to the Ohmic losses. As seen from Fig. 7(b), for the right-circularly polarized dipole the positions of peaks appear at $k_x/k_0 = -1.033$ and $k_x/k_0 = 1.094$. Conversely, for the left-circularly polarized dipole the positions of peaks appear at $k_x/k_0 = -1.094$ and $k_x/k_0 = 1.033$. The ratio between the lower and the higher intensities is 0.2494. The spectra is not strictly symmetric along the $k_x = 0$. In Fig. 7(b), the positions corresponding to the intensity peaks are at about $k_x/k_0 = \pm 1.171$ and $k_x/k_0 = \pm 1.072$ for the x-polarized and z-polarized dipoles, respectively. Moreover, from Figs. 7(c)–7(f), we can find that the x-polarized dipole leads to a much broader linewidth behavior than the z-polarized dipole.

VI. INFLUENCE OF THE DISTANCE OF THE DIPOLE ON CHIRALITY

The influence of the distance (d_1) for the dipole from the first sliver surface on the electric field distribution under the excitation of circularly polarized dipoles ($\mathbf{p}_+$ and $\mathbf{p}_-$) are considered. In Fig. 8, it can be seen that when we increase the distance d_1, the intensity spectra have a blueshift, and the asymmetry becomes obvious. By taking the right circularly polarized excitation (solid curves) for an example, the intensity of the positive peak becomes higher; inversely, the intensity of the negative peak becomes lower. At the position $k_x/k_0 = 1.088$ for $d_1 = 10$ nm, we can get $C = 0.189$, $C_x = 6.2075$, and $C_z = 0.9738$. It means that the overall energy coupling into the surface modes for circularly polarized cases is larger than that in the x-linearly polarized case, and smaller

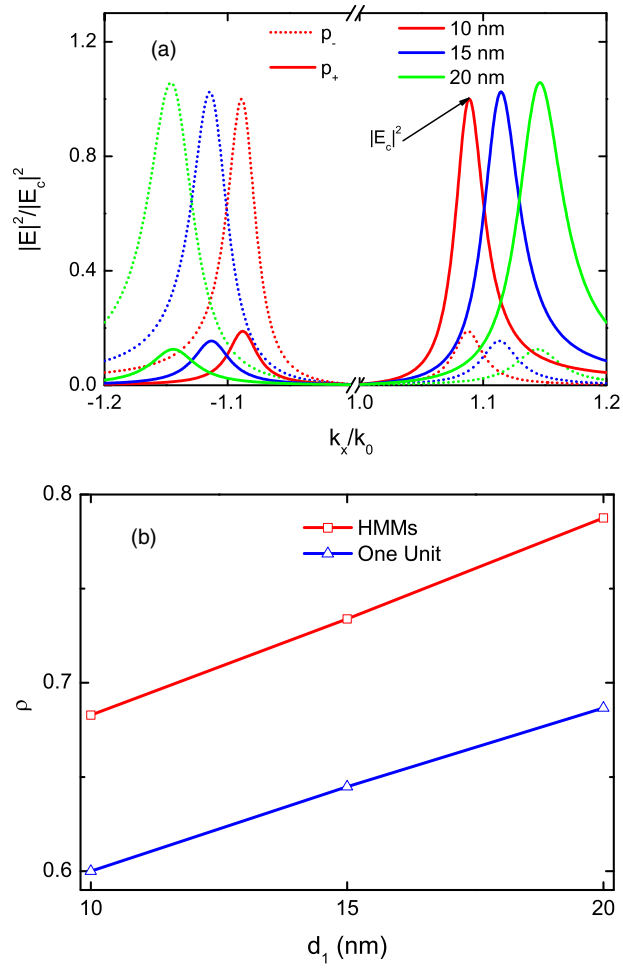

FIG. 8. (a) Plot of $|E|^2/|E_c|^2$ as a function of the wave vector component k_x excited by the right ($\mathbf{p}_+$, solid curves) and left ($\mathbf{p}_-$, dotted curves) circularly polarized dipoles. The thickness of the first Al_2O_3 layer is varied for $d_1 = 10$ nm, $d_1 = 15$ nm, and $d_1 = 20$ nm. (b) Plot of the chirality versus the distance. Here, $k_y = 0$.

than that in the z-linearly polarized case. The contribution of z component is larger than that of x component.

In order to explain the effects of the distance d_1 on the chiral emission clearly, we define the chirality parameter for $k_x > k_0$ as

$$\rho = \frac{I_m(\mathbf{p}_+) - I_m(\mathbf{p}_-)}{I_m(\mathbf{p}_+) + I_m(\mathbf{p}_-)}, \tag{13}$$

where I_m is the local maximum value induced by the corresponding dipole. The value can be changed from 0 to 1. The value $\rho = 0$ corresponds to a linear polarization without preference in the forward or backward propagating direction; while $\rho = 1$ implies a truly unidirectional excitation of the electromagnetic wave. We obtain that $\rho = 0.6829$ for $d_1 = 10$ nm, $\rho = 0.7338$ for $d_1 = 15$ nm, and $\rho = 0.7376$ for $d_1 = 20$ nm, as shown in Fig. 8(b). By increasing the distance d_1, the chirality is greatly enhanced. It is more interesting to find that for the HMMs the chirality is better than that for the single sliver film (one unit structure), even though the total thickness is much larger. This is because the HMMs have increased density of states. Therefore, we can conclude

that this directional behavior is general and can occur in the nanostructure with evanescent tails coupling to an elliptic dipolar emitter.

VII. CONCLUSIONS

In summary, we have provided a comprehensive theoretical study of directional emission by using an elliptically polarized dipole coupled to a dielectric-metal multilayered structure. The spatial frequency spectra of electric field can be obtained by using a rigorous method of photon Green's function. The presence of a circularly polarized dipole breaks the inversion symmetry of the system and enables spin-dependent directional coupling where the intensity is suppressed in one direction. This effect has been illustrated by using the hyperbolic metamaterial structure. The directional emission characteristics at HMM are much more pronounced than that on a metallic film. Furthermore, by controlling the distance of the dipole from the HMM, the chirality can be enhanced. The truly unidirectional emission requires the dipole with strong complex elliptic polarization. The near-field coherent interference between the transverse and longitudinal polarized components of the dipole lies at the heart of this work. These findings may serve as a new platform to control the excitation and guiding of surface waves and can have potential applications in sensing [63,64].

ACKNOWLEDGMENTS

G.S.A. acknowledges Dr. J. Basu for extensive discussions on his experiments about the coupling of quantum dots with HMMs. G.S.A. thanks the support from the Welch Foundation (No. A-1943-20180324). W.L. and S.G. were supported by the National Natural Science Foundation of China (NSFC) (Nos. 11534008, 91536115), and the Natural Science Foundation of Shaanxi Province (No. 2016JM1005). V.M.M. was supported through NSF Grant No. DMR-1709996.

[1] P. Lodahl, S. Mahmoodian, S. Stobbe, A. Rauschenbeutel, P. Schneeweiss, J. Volz, H. Pichler, and P. Zoller, Chiral quantum optics, Nature (London) **541**, 473 (2017).

[2] I. Shomroni, S. Rosenblum, Y. Lovsky, O. Bechler, G. Guendelman, and B. Dayan, All-optical routing of single photons by a one-atom switch controlled by a single photon, Science **345**, 903 (2014).

[3] M. Scheucher, A. Hilico, E. Will, J. Volz, and A. Rauschenbeutel, Quantum optical circulator controlled by a single chirally coupled atom, Science **354**, 1577 (2016).

[4] I. Söllner, S. Mahmoodian, S. L. Hansen, L. Midolo, A. Javadi, G. Kiršanskė, T. Pregnolato, H. El-Ella, E. H. Lee, J. D. Song, S. Stobbe, and P. Lodahl, Deterministic photon-emitter coupling in chiral photonic circuits, Nat. Nanotechnol. **10**, 775 (2015).

[5] H. Pichler, T. Ramos, A. J. Daley, and P. Zoller, Quantum optics of chiral spin networks, Phys. Rev. A **91**, 042116 (2015).

[6] W. Ma, L. Xu, L. Wang, C. Xu, and H. Kuang, Chirality-Based biosensors, Adv. Funct. Mater. **29**, 1805512 (2019).

[7] A. Hayat, J. P. Balthasar Mueller, and F. Capasso, Lateral chirality-sorting optical forces, Proc. Natl. Acad. Sci. USA **112**, 13190 (2015).

[8] J. Petersen, J. Volz, and A. Rauschenbeutel, Chiral nanophotonic waveguide interface based on spin-orbit interaction of light, Science **346**, 67 (2014).

[9] R. Mitsch, C. Sayrin, B. Albrecht, P. Schneeweiss, and A. Rauschenbeutel, Quantum state-controlled directional spontaneous emission of photons into a nanophotonic waveguide, Nat. Commun. **5**, 5713 (2014).

[10] J. Lin, J. P. B. Mueller, Q. Wang, G. Yuan, N. Antoniou, X.-C Yuan, and F. Capasso, Polarization-controlled tunable directional coupling of surface plasmon polaritons, Science **340**, 331 (2013).

[11] D. O'Connor, P. Ginzburg, F. J. Rodríguez-Fortuño, G. A. Wurtz, and A. V. Zayats, Spin-orbit coupling in surface plasmon scattering by nanostructures, Nat. Commun. **5**, 5327 (2014).

[12] F. J. Rodríguez-Fortuño, G. Marino, P. Ginzburg, D. O'Connor, A. Martínez, G. A. Wurtz, and A. V. Zayats, Near-feld interference for the unidirectional excitation of electromagnetic guided modes, Science **340**, 328 (2013).

[13] N. Shitrit, I. Yulevich, E. Maguid, D. Ozeri, D. Veksler, V. Kleiner, and E. Hasman, Spin-optical metamaterial route to spin-controlled photonics, Science **340**, 724 (2013).

[14] X. Yin, Z. Ye, J. Rho, Y. Wang, and X. Zhang, Photonic spin Hall effect at metasurfaces, Science **339**, 1405 (2013).

[15] K. Y. Bliokh, Y. Gorodetski, V. Kleiner, and E. Hasman, Coriolis Effect in Optics: Unified Geometric Phase and Spin-Hall Effect, Phys. Rev. Lett. **101**, 030404 (2008).

[16] P. V. Kapitanova, P. Ginzburg, F. J. Rodríguez-Fortuño, D. S. Filonov, P. M. Voroshilov, P. A. Belov, A. N. Poddubny, Y. S. Kivshar, G. A. Wurtz, and A. V. Zayats, Photonic spin Hall effect in hyperbolic metamaterials for polarization-controlled routing of subwavelenth modes, Nat. Commun. **5**, 3226 (2014).

[17] K. Y. Bliokh, A. Y. Bekshaev, and F. Nori, Extraordinary momentum and spin in evanescent waves, Nat. Commun. **5**, 3300 (2014).

[18] T. Van Mechelen and Z. Jacob, Universal spin-momentum locking of evanescent waves, Optica **3**, 118 (2016).

[19] I. S. Sinev, A. A. Bogdanov, F. E. Komissarenko, K. S. Frizyuk, M. I. Petrov, I. S. Mukhin, S. V. Makarov, A. K. Samusev, A. V. Lavrinenko and I. V. Iorsh, Chirality driven by magnetic dipole response for demultiplexing of surface waves, Laser Photon. Rev. **11**, 1700168 (2017).

[20] C. L. Cortes, W. Newman, S. Molesky and Z. Jacob, Quantum nanophotonics using hyperbolic metamaterials, J. Opt. **14**, 063001 (2012).

[21] L. Lu, R. E. Simpson, and S. K. Valiyaveedu, Active hyperbolic metamaterials: Progress, materials and design, J. Opt. **20**, 103001 (2018).

[22] A. Nemilentsau, T. Stauber, G. Gómez-Santos, M. Luskin, and T. Low, Switchable and unidirectional plasmonic beacons in hyperbolic two-dimensional materials, Phys. Rev. B **99**, 201405 (2019).

[23] S. A. Hassani Gangaraj, G. W. Hanson, M. G. Silveirinha, K. Shastri, M. Antezza, and F. Monticone, Unidirectional and

diffractionless surface plasmon polaritons on three-dimensional nonreciprocal plasmonic platforms, Phys. Rev. B **99**, 245414 (2019).

[24] I. I. Smolyaninov and E. E. Narimanov, Metric Signature Transitions in Optical Metamaterials, Phys. Rev. Lett. **105**, 067402 (2010).

[25] Z. Jacob, I. I. Smolyaninov, and E. E. Narimanov, Broadband purcell effect: Radiative decay engineering with metamaterials, Appl. Phys. Lett. **100**, 181105 (2012).

[26] A. N. Poddubny, P. A. Belov, and Y. S. Kivshar, Spontaneous radiation of a finite-size dipole emitter in hyperbolic media, Phys. Rev. A **84**, 023807 (2011).

[27] A. S. Potemkin, A. N. Poddubny, P. A. Belov, and Y. S. Kivshar, Green function for hyperbolic media, Phys. Rev. A **86**, 023848 (2012).

[28] O. Kidwai, S. V. Zhukovsky, and J. E. Sipe, Effective-medium approach to planar multilayer hyperbolic metamaterials: Strengths and limitations, Phys. Rev. A **85**, 053842 (2012).

[29] I. Iorsh, A. Poddubny, A. Orlov, P. Belov, and Y. S. Kivshar, Spontaneous emission enhancement in metal-dielectric metamaterials, Phys. Lett. A **376**, 185 (2012).

[30] O. Kidwai, S. V. Zhukovsky, and J. E. Sipe, Dipole radiation near hyperbolic metamaterials: Applicability of effective-medium approximation, Opt. Lett. **36**, 2530 (2011).

[31] A. A. Orlov, P. M. Voroshilov, P. A. Belov, and Y. S. Kivshar, Engineered optical nonlocality in nanostructured metamaterials, Phys. Rev. B **84**, 045424 (2011).

[32] J. Kim, V. P. Drachev, Z. Jacob, G. V. Naik, A. Boltasseva, E. E. Narimanov, and V. M. Shalaev, Improving the radiative decay rate for dye molecules with hyperbolic metamaterials, Opt. Express **20**, 8100 (2012).

[33] H. N. S. Krishnamoorthy, Z. Jacob, E. Narimanov, I. Kretzschmar, and V. M. Menon, Topological transitions in metamaterials, Science **336**, 205 (2012).

[34] T. Galfsky, H. N. S. Krishnamoorthy, W. Newman, E. E. Narimanov, Z. Jacob, and V. M. Menon, Active hyperbolic metamaterials: Enhanced spontaneous emission and light extraction, Optica **2**, 62 (2015).

[35] Y. Wang, H. Sugimoto, S. Inampudi, A. Capretti, M. Fuji, and L. Dal Negro, Broadband enhancement of local density of states using silicon-compatible hyperbolic metamaterials, Appl. Phys. Lett. **106**, 241105 (2015).

[36] Z. Jacob, L. V. Alekseyev, and E. Narimanov, Optical hyperlens: Far-field imaging beyond the diffraction limit, Opt. Express **14**, 8247 (2006).

[37] D. R. Smith, P. Kolinko, and D. Schurig, Negative refraction in indefinite media, J. Opt. Soc. Am. B **21**, 1032 (2004).

[38] A. J. Hoffman, L. Alekseyev, S. S. Howard, K. J. Franz, D. Wasserman, V. A. Podolskiy, E. E. Narimanov, D. L. Sivco, and C. Gmachl, Negative refraction in semiconductor metamaterials, Nat. Mater. **6**, 946 (2007).

[39] A. A. High, R. C. Devlin, A. Dibos, M. Polking, D. S. Wild, J. Perczel, N. P. de Leon, M. D. Lukin, and H. Park, Visible-frequency hyperbolic metasurface, Nature (London) **522**, 192 (2015).

[40] S.-A. Biehs, V. M. Menon, and G. S. Agarwal, Long-range dipole-dipole interaction and anomalous Förster energy transfer across a hyperbolic metamaterial, Phys. Rev. B **93**, 245439 (2016).

[41] C. L. Cortes and Z. Jacob, Super-Coulombic atom-atom interactions in hyperbolic media, Nat. Commun. **8**, 14144 (2017).

[42] W. D. Newman, C. L. Cortes, and Z. Jacob, Enhanced and directional single-photon emission in hyperbolic metamaterials, J. Opt. Soc. Am. B **30**, 766 (2013).

[43] A. N. Poddubny, P. A. Belov, P. Ginzburg, A. V. Zayats, and Y. S. Kivshar, Microscopic model of Purcell enhancement in hyperbolic metamaterials, Phys. Rev. B **86**, 035148 (2012).

[44] W. Yan, M. Wubs, and N. A. Mortensen, Hyperbolic metamaterials: Nonlocal response regularizes broadband supersingularity, Phys. Rev. B **86**, 205429 (2012).

[45] Y. Yermakov, A. I. Ovcharenko, A. A. Bogdanov, I. V. Iorsh, K. Y. Bliokh, and Y. S. Kivshar, Spin control of light with hyperbolic metasurfaces, Phys. Rev. B **94**, 075446 (2016).

[46] T. Chervy, S. Azzini, E. Lorchat, S. Wang, Y. Gorodetski, J. A. Hutchison, S. Berciaud, T. W. Ebbesen, and C. Genet, Room temperature chiral coupling of valley excitons with spin-momentum locked surface plasmons, ACS Photon. **5**, 1281 (2018).

[47] S. Guddala, R. Bushati, M. Li, A. B. Khanikaev, and V. M. Menon, Valley selective optical control of excitons in 2D semiconductors using a chiral metasurface [Invited], Opt. Mater. Exp. **9**, 536 (2019).

[48] L. Sun, C. Y. Wang, A. Krasnok, J. Choi, J. Shi, J. S. G. Diaz, A. Zepeda, S. Gwo, C. K. Shih, A. Alú, and X. Li, Separation of valley excitons in a MoS_2 monolayer using a subwavelength asymmetric groove array, Nat. Photon. **13**, 180 (2018).

[49] O. Bitton, S. N. Gupta, and G. Haran, Quantum dot plasmonics: From weak to strong coupling, Nanophotonics **8**, 559 (2019).

[50] P. K. Jha, N. Shitrit, X. Ren, Y. Wang, and X. Zhang, Spontaneous Exciton Valley Coherence in Transition Metal Dichalcogenide Monolayers Interfaced With an Anisotropic Metasurface, Phys. Rev. Lett. **121**, 116102 (2018).

[51] S. Guddala, M. Khatoniar, N. Yama, and V. M. Menon, Optical valley-Hall effect of 2D excitons, Conference on Lasers and Electro-Optics, OSA Tec. Dig., Optical Society of America, 2019, paper FM4D.2.

[52] Jaydeep Basu (private communication).

[53] G. S. Agarwal, Interaction of electromagnetic waves at rough dielectric surfaces, Phys. Rev. B **15**, 2371 (1977).

[54] O. Takayama, L. C. Crasovan, S. K. Johansen, D. Mihalache, D. Artigas, and L. Torner, Dyakonov surface waves: A review, Electromagnetics **28**, 126 (2008).

[55] O. Y. Yermakov, A. A. Hurshkainen, D. A. Dobrykh, P. V. Kapitanova, I. V. Iorsh, S. B. Glybovski, and A. A. Bogdanov, Experimental observation of hybrid TE-TM polarized surface waves supported by a hyperbolic metasurface, Phys. Rev. B **98**, 195404 (2018).

[56] L. Novotny and B. Hecht, *Principles of Nano-Optics* (Cambridge University Press, Cambridge, 2012).

[57] P. Shekhar, J. Atkinson, and Z. Jacob, Hyperbolic metamaterials: Fundamentals and applications, Nano Converg. **1**, 14 (2014).

[58] S. V. Zhukovsky, O. Kidwai, and J. E. Sipe, Physical nature of volume plasmon polaritons in hyperbolic metamaterials, Opt. Express **21**, 14982 (2013).

[59] M. Tschikin, S.-A. Biehs, R. Messina, and P. Ben-Abdallah, On the limits of the effective description of hyperbolic materials in the presence of surface waves, J. Opt. **15**, 105101 (2013).

[60] K. Y. Bliokh and F. Nori, Transverse spin of a surface polariton, Phys. Rev. A **85**, 061801 (2012).

[61] K. Y. Bliokh, D. Smirnova, and F. Nori, Quantum spin Hall effect of light, Science **348**, 1448 (2015).

[62] O. Takayama, J. Sukham, R. Malureanu, A. V. Lavrinenko, and G. Puentes, Photonic spin Hall effect in hyperbolic metamaterials at visible wavelengths, Opt. Lett. **43**, 4602 (2018).

[63] N. Bourg, C. Mayet, G. Dupuis, T. Barroca, P. Bon, S. Lécart, E. Fort, and S. Lévêque-Fort, Direct optical nanoscopy with axially localized detection, Nat. Photon. **9**, 587 (2015).

[64] Q. Ma, H. Qian, S. Montoya, W. Bao, L. Ferrari, H. Hu, E. Khan, Y. Wang, E. E. Fullerton, E. E. Narimanov, X. Zhang, and Z. Liu, Experimental demonstration of hyperbolic metamaterial assisted illumination nanoscopy, ACS Nano. **12**, 11316 (2018).